Journal of Membrane Science 488 (2015) 121–128

Contents lists available at ScienceDirect

Journal of Membrane Science

journal homepage: www.elsevier.com/locate/memsci

Hybrid silica membranes with enhanced hydrogen and CO_2 separation properties

Hessel L. Castricum [a,b], Hammad F. Qureshi [a], Arian Nijmeijer [a], Louis Winnubst [a,*]

[a] Inorganic Membranes, MESA+ Institute for Nanotechnology, University of Twente, P. O. Box 217, 7500AE Enschede, The Netherlands
[b] Van 't Hoff Institute for Molecular Sciences, University of Amsterdam, Science Park 904, 1098 XH Amsterdam, The Netherlands

ARTICLE INFO

Article history:
Received 22 January 2015
Received in revised form
13 March 2015
Accepted 22 March 2015
Available online 20 April 2015

Keywords:
Hybrid silica
Sol–gel processing
In-situ SAXS
Microporous membrane
Gas separation

ABSTRACT

Hybrid silica membranes are of great interest for molecular separation owing to their outstanding hydrothermal stability. Despite good separation properties in liquid applications, the selectivity for gas separations has yet been too low. Here, we report membranes from 1,2-*bis*(triethoxysilyl)ethane (BTESE) with H_2/N_2 permselectivity between 50 and over 400. The membranes are fabricated from a dip-sol with a H^+:Si ratio of 0.01 that is applied onto a support system with a controlled low water content (pre-treated at RH < 0.5%). For support systems pre-treated at 90% RH, H_2/N_2 permselectivities ≤ 10 are obtained, indicating larger pores. The pore formation process is studied *in situ* by Small-Angle X-ray Scattering in a dedicated setup. The formation of larger pores can be understood by a higher condensation rate and longer drying times when more water is present. This results in a stronger network that better withstands the compressive forces during drying. By limiting both the water and acid contents in the dipped sol, a dense pore structure is obtained that gives the highest H_2/N_2 and CO_2/CH_4 permselectivities found to date for hybrid silica membranes. Further variation of the water and acid concentration will allow for additional tuning of the separation properties for both gas and liquid separation.

© 2015 Elsevier B.V. All rights reserved.

1. Introduction

The separation and purification of molecular mixtures in the chemical industry consume substantial amounts of energy. To reduce fossil fuel consumption, efficient separation processes are needed to obtain high-grade products in the food and pharmaceutical industries [1,2], high-purity water [3], and to remove or recover toxic or valuable components from industrial effluents [4]. Today, membranes are used on a large scale for the production of potable water, cleaning industrial effluents, recovering valuable constituents in biomass fermentation [5–7], biogas upgrading [8] and for gas and vapor separation [9,10]. Besides, membranes are a key component in energy conservation and -storage systems [11], artificial organs [12] and drug delivery devices [13].

Amorphous silica is an attractive material for the application in microporous inorganic membranes because of its thermal stability and high gas separation selectivity [14]. Through acid catalyzed sol–gel processing of *e.g.* tetraethylorthosilicate (TEOS), it is relatively easy to develop a thin separation layer with a narrow pore size that is applied onto a support that provides mechanical strength [15]. After thermal consolidation of the dip-coated sol-gel-derived silica network, a homogeneous membrane is formed [16] that allows the selective permeation of small molecules such as helium (kinetic diameter = 0.26 nm) and hydrogen (0.289 nm), while showing little or no permeation of the bigger molecules like nitrogen (0.364 nm) or methane (0.389 nm) [17]. However, the low stability of the silica structure to water severely limits its application in many industrial processes that involve hydrothermal conditions [18]. Modification of the silica network with metal ions [19–22] or the use of silanes with hydrophobicity-inducing pendant alkyl groups [18,23,24] have been reported to improve the hydrothermal stability.

An even more effective way to obtain high hydrothermal stability is by applying silicon alkoxide precursors that contain an organic bridging group between two silicon atoms [25–30], such as 1,2-*bis*(triethoxysilyl)ethane (BTESE). Acid-catalyzed hydrolysis and condensation of BTESE can be assumed to follow the same S_N2-reaction mechanism as for tetraalkoxysilanes [31–33]. A single dipping procedure allows the formation of an isotropic selective layer with a homogenous pore microstructure, with reported thicknesses down to 90 nm [29]. The resulting 'hybrid silica' membrane has shown stability in relevant liquid mixtures with water for several years at 150 °C and higher [25,34]. The exceptional hydrothermal stability of hybrid silica has directly been associated

* Corresponding author. Tel.: +31 53 4892994; fax: +31 53 4892336.
E-mail address: a.j.a.winnubst@utwente.nl (L. Winnubst).

http://dx.doi.org/10.1016/j.memsci.2015.03.084
0376-7388/© 2015 Elsevier B.V. All rights reserved.

with the organic bridging group. This provides a higher internal network connectivity of the minimum non-hydrolyzable 'building block', and enhances the mechanical properties, which results in a lower sensitivity of Si–O–Si to hydrolysis, and in a higher fracture resistance [35]. By varying the structure of the organic bridge, different separation properties can be obtained [28]. Short alkylene bridging groups were found to be advantageous for separations based on differences in molecular size, while separation based on differences in the affinity of adsorption in the material were enhanced for membranes with longer (C_8H_{16}) alkylene and aryl bridges. Recently, it was shown that the pore size can be varied independently by applying different acid contents previous to drying [36]. By adding more acid catalyst, larger pores are formed, which gives higher overall permeances and allows the separation of mixtures of larger molecules. At low acid content, the H_2O/butanol pervaporation selectivity was improved. By reducing the H^+:Si ratio (acid ratio, AR) from 0.1 to 0.01, a tenfold increase of the H_2O separation factor to $7.9 \cdot 10^3$ was measured. However, lowering AR below 0.1 did not result in a better gas permselectivity. H_2/N_2 and H_2/CH_4 permselectivities were limited to about 25 for BTESE-derived membranes, suggesting a lower limit in the pore size. Values reported by various groups for this type of membrane are all of the same order (Table 1). Computer simulations indicated that the lower permselectivities as compared to those reported for SiO_2 are related to the size of the bridging group [37,38]. This could explain the substantial permeation of molecules of the size of N_2.

Acid-catalyzed sol–gel synthesis of silica results in sols with linear polymeric chains, giving microporous materials after drying and calcination [16]. The smallest pores are produced around the isoelectric point (pH ≈ 2), at which condensation rates are at a minimum. Compressive capillary forces exerted by the receding pore liquid may determine the pore structure formed during drying [36]. With more acid, the compressive forces are balanced by a network strengthened by ongoing condensation reactions, and by the positive charge on the hybrid organosilica. This results in larger pores. We investigate here whether the presence of additional water, which is a reactant in sol–gel hydrolysis and condensation, may similarly give larger pores. Water present in the mesopores of the support system may diffuse into the applied sol. We investigated the role of water by pretreating the membrane supports before the dip-coating process in different atmospheres of controlled humidity. It was anticipated that narrower pores could be formed with a smaller amount of water in the support, giving a higher size selectivity to gas permeation. Membranes were prepared at AR = 0.01 and 0.1, and additional experiments were carried out for unsupported systems to study the pore formation process *in situ*. Considering the general complexity of the membrane preparation process, results on the membrane with the highest permselectivity were reproduced multiple times to ensure that the results were not accidental. Because of their high hydrothermal stability, hybrid silica membranes with high and tunable gas separation selectivity could prove of great promise for application, as realistic gas mixtures are usually not strictly devoid of water.

Table 1
Reported highest H_2/N_2 permeation ratios for BTESE-based organosilica membranes, along with the H^+:Si acid ratios (AR) and consolidation temperatures (*T*).

AR	*T*	H_2/N_2 permselectivity	Ref.
0.1	523	27	[36]
0.08	473	15	[45]
0.05	473	10	[27]
0.05	473	20	[46]
0.05	473	34	[47]
0.05	473	40	[48]

2. Experimental

1,2-*bis*(triethoxysilyl)ethane (BTESE) (purity 97%, ABCR Germany) was used as a hybrid silica precursor. Water was deionized at 18.2 MΩ/cm using a Millipore purification system. A polymeric sol was prepared by drop-wise addition of BTESE to a nitric acid (65 wt%, Aldrich)–water–dry ethanol mixture. Nitric acid has been used for the preparation of many other silica-based sol systems applied for membranes. Addition was done in an ice bath under vigorous stirring to control the reaction rate and thus avoid extensive early-stage hydrolysis. This mixture was subsequently refluxed at 333 K under continuous stirring to produce a hybrid silica sol at H^+:Si (acid ratio, AR) = 0.01 and H_2O:–OC_2H_5 (hydrolysis ratio, HR, with –OC_2H_5 the hydrolysable alkoxy-group in the BTESE precursor) = 1. A second sol was prepared with AR = 0.1 and HR = 1.

Membranes were synthesized by means of coating these sols on porous γ-alumina ceramic membrane support systems. These were prepared by dip-coating a boehmite–PVA sol on α-alumina supports (support thickness of 2.08 ± 0.01 mm and pore diameter of about 100 nm; Pervatech B.V. The Netherlands), followed by subsequent drying and calcination, as described in detail in [15]. The dip-sol was applied twice to create a smooth mesoporous γ-alumina intermediate layer with 3–5 nm pore diameter, as determined with permporometry [39].

For membrane fabrication, the BTESE sol was diluted to a final dip-sol with [Si] = 0.6 M. This dip-sol was applied onto the alumina support system by a single dipping procedure (withdrawal rate 1.4 cm/s) in a class 100 flow cupboard situated in a class 1000 cleanroom (controlled at 296–298 K and RH = 45–55%), followed by a thermal treatment at 573 K for 3 h in N_2 (99.99% pure) with heating and cooling rates of 0.5 K/min. Prior to coating, the support was either kept in a furnace at 413 K for 24 h (relative humidity, RH < 0.5%) or in a climate chamber at 348 K at RH = 90% for 72 h. The thicknesses of the hybrid silica top-layer of the membranes were determined from cross-sectional micrographs acquired with a high-resolution scanning electron microscope HR-SEM (ZEIS 1550) at an accelerating voltage of 1.0 kV. Unsupported xerogels were prepared by drying and a thermal treatment under the same conditions as for the supported membranes.

Particle sizes of freshly prepared hybrid sols were determined by dynamic light scattering (DLS) using a Malvern Zetasizer Nano ZS at 298 K. The hydrodynamic diameter of the sol particles was determined from the Brownian motion of the particles as defined by the translational diffusion coefficient *D* in the ethanol solvent. The hydrodynamic diameter d_{hyd} was obtained by the Stokes–Einstein equation

$$d_{hyd} = kT/3\pi\eta D \tag{1}$$

in which *k* is Boltzmann's constant, *T* is the temperature, η is the solvent viscosity and *D* is the diffusion coefficient in the solvent.

N_2 adsorption/desorption isotherms were obtained for unsupported xerogels on a CE-Instruments Milestone 200 at 77 K after drying ($p < 10^{-4}$ mbar at 473 K). Surface areas were determined by the Dubinin method, modified by Kaganer [40,41], as in

$$\log n = \log n_m + D_a(\log p^0/p)^2 \tag{2}$$

with *n* is the gas adsorbed at relative pressure p/p^0, n_m is the monolayer capacity of the surface, both expressed in mol per g adsorbent, and D_a is an adsorbent-dependent constant. The surface areas *A* were subsequently determined according to

$$A = n_m a_m N_A \tag{3}$$

in which N_A is Avogadro's number and a_m is the area occupied by a molecule in the completed monolayer, taken as 0.162 nm^2 for N_2 (ISO 9277). The mean pore diameter d_p was calculated from the

pore volume v_p, determined at $p/p^0=0.98$, and the surface area A, assuming cylindrical pores

$$d_p = 4v_p/A \quad (4)$$

Small-angle X-ray scattering (SAXS) measurements were carried out at the DUBBLE beamline BM-26B [42] of the European Synchrotron Radiation Facility in Grenoble, France. Scattering data were obtained using 16 keV X-rays. The samples were placed at a distance of 1.5 m from the detector and the intensity was measured with a 2D gas-filled detector. The raw data were corrected for the pixel-dependent detector sensitivity and integrated for channels with the same q values. *In-situ* drying experiments were carried out at 333 K by using a specially designed set-up consisting of a vertically rotating cylinder covered with Kapton foil [43], in which the liquid sol was contained by means of centrifugal force. 5 ml of a sol was introduced to produce a liquid layer with a thickness of 1 mm. Scattering patterns were acquired at time intervals of 2 min to follow the drying process of the sol in the rotating cylinder. Measurements on thermally consolidated xerogel samples were obtained by applying them onto a Kapton foil. The scattering pattern of a clean foil under the same conditions was used for background correction.

Gas permeation properties were determined in an in-house designed single gas permeation (SGP) set-up in a dead-end mode with atmospheric backpressure. The membranes were sealed in a stainless steel module using Viton® 51414 O-rings with the separation layer exposed to the feed side. The gas permeance of He (0.26 nm), H_2 (0.289 nm), CO_2 (0.33 nm), N_2 (0.364 nm), CH_4 (0.389 nm) to SF_6 (0.55 nm) was measured in a sequence, starting with the gas of smallest kinetic diameter, at 473 K and 3 bar feed pressure. This temperature was chosen to balance low surface adsorption of gases and vapors and avoiding thermal membrane degradation. The pressure difference over the membrane was measured by a differential pressure sensor (GE Druck STX2100). The flow through the membrane was determined by a Bronkhorst EL-FLOW mass flow meter. Low permeances were double-checked with a soap bubble method. After the measuring sequence, the hydrogen permeance was determined again to ensure that no microstructural changes had occurred in the membrane during the measurements.

The permeance F_i of gas i was determined from

$$F_i = N_i/S_m\Delta p \quad (5)$$

with N_i is the gas flux through the membrane, S_m is the exposed membrane surface area and Δp is the pressure difference (2 bar) between the feed and permeate sides.

3. Results and discussion

3.1. Sol preparation and membrane structure

For preparation of the dip-sol, the synthesis procedure was adapted to obtain a mean particle size of 7 nm. This is well above the 4 nm pore size of the γ-alumina support layer [39], precluding extensive penetration into the support, and below 15 nm, above which the sols become polydisperse [28]. Sols with large particles also tend to form thick layers that are prone to cracking [44]. While the hydrolysis and condensation rates increase with reactant concentration, a similar sol structure can still be achieved by adjusting the synthesis time. In view of manageability of the coating sol, the latter was aimed at being in the order of hours. By applying [Si]=2.7 M and 1.8 M, respectively, fine-tuning of the synthesis time resulted in very similar sols at AR=0.01 and 0.1 with the desired properties (Fig. 1). This guaranteed optimal and very comparable coating conditions. Both sols were below the isoelectric point of silica, which is around pH=2 in an aqueous medium [16,36]. Such acid-catalyzed conditions are required to obtain a microporous structure. Base-catalyzed systems would rather lead to mesopores that are undesirable for size-selective gas and vapor separation. After dilution with ethanol to [Si]=0.6 M, the sol was immediately dip-coated onto γ-alumina support systems. Subsequently, the membranes were thermally treated to consolidate the structure. Cross-sectional high-resolution scanning electron micrographs indicate that the membranes from the sols with AR=0.1 and 0.01 are isotropic with thicknesses of similar dimensions, *i.e.* around 0.5 μm (Fig. 2). This confirms that the sol properties were sufficiently similar to produce layers of similar thickness.

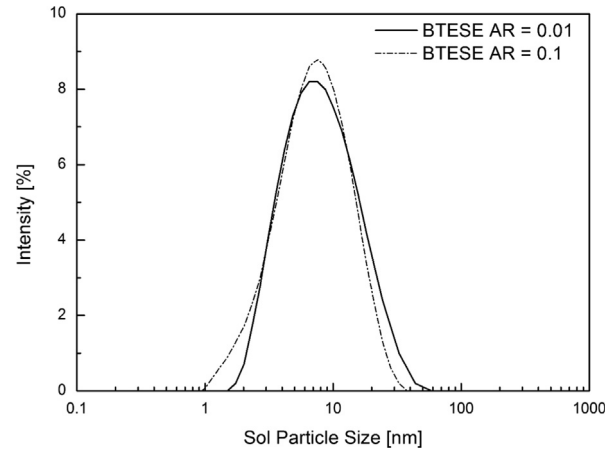

Fig. 1. Sol particle size distributions of BTESE-based sols with AR=0.01 and AR=0.1 [29], determined with dynamic light scattering.

3.2. Membrane behavior in gas permeation

3.2.1. Membranes prepared on a dry support

Single gas permeation results on hybrid silica membranes prepared on supports that were well dried (RH < 0.5% at 413 K) prior to coating are given in Table 2. Considering the very low N_2 and CH_4 permeances for the AR=0.01 membranes, the full procedure of sol preparation and membrane synthesis was repeated several times to ensure the validity of the results. For all membranes, the SF_6 permeance was below the detection limit of the equipment of $5\cdot10^{-10}$ mol m^{-2} s^{-1} Pa^{-1}, indicating that the microstructure contained very few defects. For two of the four synthesized AR=0.01 membranes, the nitrogen and methane permeances were also below the $5\cdot10^{-10}$ mol m^{-2} s^{-1} Pa^{-1} detection limit. For the third membrane, no detectable methane permeance was observed, while a N_2 permeance of $3\cdot10^{-9}$ mol m^{-2} s^{-1} Pa^{-1} resulted in a H_2/N_2 permselectivity of 80. A fourth membrane showed H_2/N_2 and H_2/CH_4 permselectivities of respectively 50 and 88. The H_2 permeances were all in a narrow range between 1.88 and $2.38\cdot10^{-7}$ mol m^{-2} s^{-1} Pa^{-1}. While the spread in especially the low permeances of the larger gases observed for the AR=0.01 membranes could be related to the presence of a small fraction of somewhat larger pores, the difference with the AR=0.1 membrane is substantial, indicating a denser pore structure at AR=0.01. The permselectivities of the AR=0.1 membrane are more in line with those reported in earlier studies (Table 1) [27,36,45–48]. The permeances for the smaller gases He, H_2 and CO_2 for AR=0.01 were also somewhat lower than for the AR=0.1 membrane, despite the comparable thickness of the selective layer. This similarly indicates a denser pore structure. A higher measured resistance for membranes with smaller pores was also reported in Ref. [36]. The denser pore structure of the

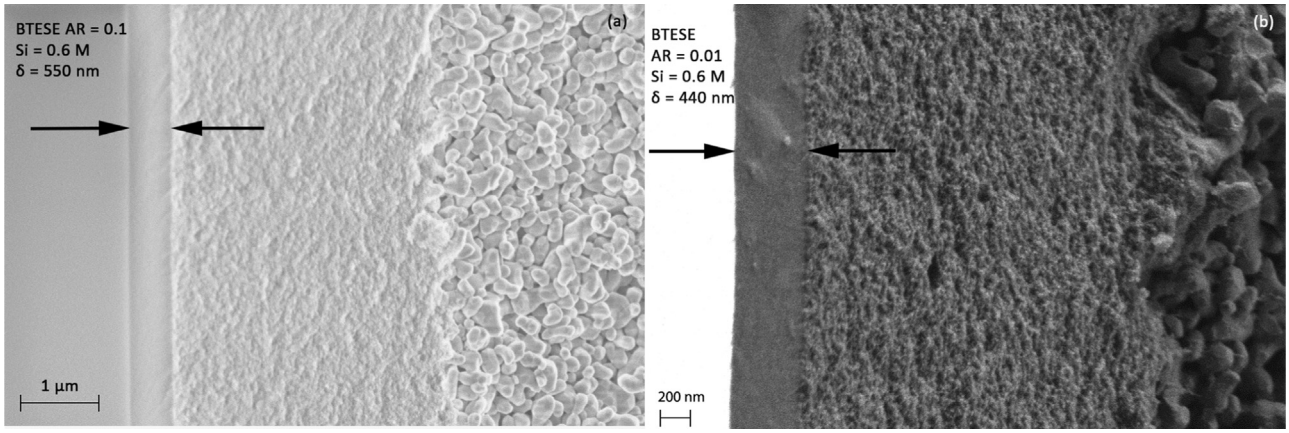

Fig. 2. Cross-sectional scanning electron micrographs of BTESE-based membranes, with the hybrid silica top layer indicated, for acid ratios (AR)=0.1 [29] (a) and 0.01 (b). The layers to the right of the top layer are the γ-alumina and α-alumina layers of the support.

Table 2
Single gas permeances (473 K, Δp=2 bar) and relevant permselectivities for hybrid silica membranes prepared from sols with AR=0.01, displayed with decreasing N_2 permeance, for a membrane prepared at AR=0.1 [29], and for the γ-alumina support system ('supp'). For the hybrid silica membranes, all supports had been pre-treated at RH < 0.5%.

	Gas permeance [10^{-9} mol m^{-2} s^{-1} Pa^{-1}]					Permselectivity				
AR	He	H_2	CO_2	N_2	CH_4	H_2/CO_2	H_2/N_2	H_2/CH_4	CO_2/N_2	CO_2/CH_4
0.01	133	188	33	3.8	2.1	6	50	88	9	15
0.01	210	238	56	3.0	[a]	4	80	[a]	19	[a]
0.01	179	221	50	[a]	[a]	4	[a]	[a]	[a]	[a]
0.01	179	210	44	[a]	[a]	5	[a]	[a]	[a]	[a]
0.1	205	270	46	13	11	6	21	24	3.5	4.2
supp	591	812	174	231	294	5	3.5	2.8	0.8	0.6

[a] N_2 or CH_4 permeance below the detection limit of $5 \cdot 10^{-10}$ mol m^{-2} s^{-1} Pa^{-1}, giving H_2/N_2 and H_2/CH_4 permselectivities > 400, CO_2/N_2 and CO_2/CH_4 permselectivities > 100.

AR=0.01 membranes is more suitable for size-selective separation of gas molecules.

The high H_2/N_2 permselectivities for the AR=0.01 membranes deviate clearly from those reported in [36], which were much lower for similar AR=0.01 membranes. However, as the latter membranes were prepared on supports that had been stored in ambient air (T=293 K, RH ≈ 60%) prior to dip-coating, it can be suggested that the presence of capillary water in the mesopores of the alumina support affects the pore formation process of the microporous hybrid silica layer. To investigate this, we prepared membranes onto a support that had been exposed to conditions of controlled high humidity prior to coating, as reported below.

3.2.2. Membranes prepared on a moist support

Both sols with AR=0.1 and 0.01 were coated onto supports that had been kept under 90% RH conditions at 348 K for 72 h. After thermal consolidation of the membranes, they were similarly characterized with single gas permeation. While the permeances through the AR=0.1 membrane again indicated the presence of somewhat larger pores than for AR=0.01, both membranes exhibited substantially higher N_2 and CH_4 permeances than those prepared by coating onto dry supports (Table 3). The AR=0.1 membrane even showed a SF_6 permeance clearly above the detection limit. The larger pore sizes were also reflected in the

Table 3
Single gas permeances (473 K) and relevant permselectivities for hybrid silica membranes prepared from sols with AR=0.01 and AR=0.1, with the supports pre-treated at RH=90%.

	Gas permeance [10^{-9} mol m^{-2} s^{-1} Pa^{-1}]						Permselectivity			
AR	He	H_2	CO_2	N_2	CH_4	SF_6	H_2/CO_2	H_2/N_2	H_2/CH_4	CO_2/CH_4
0.01	148	181	36.6	17.8	14.3	[a]	5	10	12	2.6
0.1	342	452	123	62.7	78.1	1.7	4	7	6	1.6

[a] SF_6 permeance below the detection limit of $5 \cdot 10^{-10}$ mol m^{-2} s^{-1} Pa^{-1}.

almost an order of magnitude lower H_2/N_2, H_2/CH_4 and CO_2/CH_4 permselectivities.

The H_2/CO_2 permselectivity was of the same order for all membranes, indicating that the permeation of CO_2 is not affected by the pore structure. As the data were acquired at 473 K, possible surface interaction effects with the Si–OH groups at the membrane surface [28,36] are small. Moreover, it can be assumed that such interactions are similar for all investigated membranes. Hence, it can be concluded that a molecular sieving effect is in effect with the cutoff between the kinetic diameters of CO_2 and N_2. The differences in pore size related to the preparation conditions therefore only affect the permeation of gas molecules larger than CO_2, *i.e.* of the size of N_2 and larger.

Fig. 3 shows the normalized single-gas permeances (F_i/F_{H_2}) of the membranes prepared on both the moist and dry supports. For the AR=0.01 membrane on the dry support, the average of all four membranes was calculated, assuming a permeance equal to the detection limit for the membranes through which no detectable gas flux was measured. The figure shows again that the permeation of gases larger than CO_2 depends on the sol–gel recipe and on the pretreatment of the support system.

While the pretreatment of the support clearly affects the porosity of the resulting hybrid silica membranes, the actual amount of water that had transpired into the freshly dipped sol cannot be determined quantitatively for nm-sized thin layers. Moreover, both adsorption of water vapor from the atmosphere into the pores of the support and diffusion into the dip-sol depend strongly on kinetic factors. We therefore verified whether the presence of additional water would also lead to larger pores in unsupported materials and investigated how the process of pore formation proceeds. To this aim, the formation of micropores was studied *in-situ* upon drying, as reported in Section 3.3.

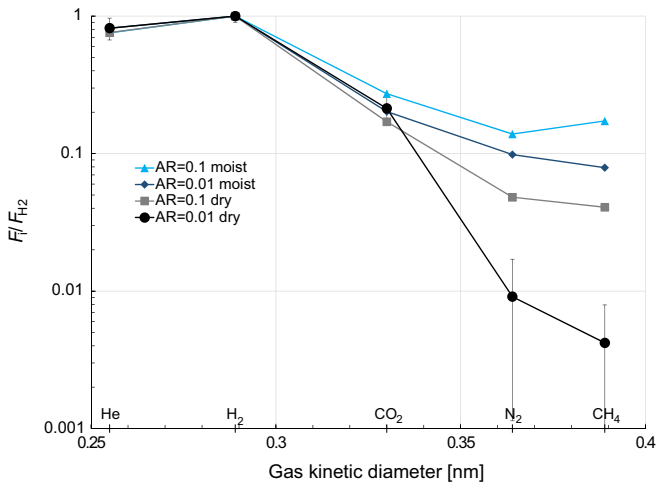

Fig. 3. Normalized single-gas permeances F_i/F_{H_2} (473 K, $\Delta p = 2$ bar) of BTESE-based membranes with AR=0.01 and AR=0.1 coated onto support systems pretreated at RH < 0.5% ('dry') and 90% ('moist'). For AR=0.01 dry, the average of the four membranes from Table 2 is displayed, with the detection limit assumed as the actual measured gas permeance in case the N_2 or CH_4 permeance was below this value. Standard deviations are given for this series.

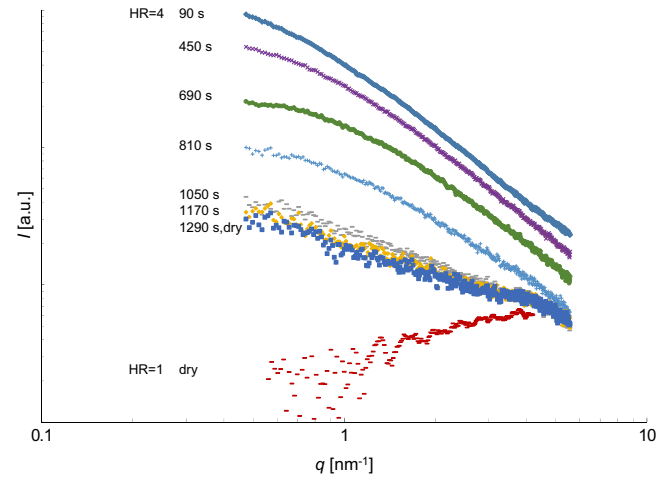

Fig. 4. SAXS patterns acquired during drying of a sol with AR=0.01 and HR=4 at the indicated drying times. The pattern of the dried material is compared to that of a dry material from a sol with AR=0.01 and HR=1 (bottom pattern, from [36]).

3.3. Pore structure of unsupported hybrid silica

SiO_2 materials from precursors such as tetraethylorthosilicate usually have a larger micropore volume and larger pores when prepared at higher HR, as observed for both unsupported materials [49–51] and membranes [52]. A higher HR also results in faster gelation of SiO_2-based sols [16], and in larger fractal dimensions and gyration radii after a specific reaction time [49,50,53,54]. The latter can be explained by the higher reactivity of these sols, as this depends on the concentration of each of the reactants. These studies also showed that increasing the acid ratio (AR) has an even stronger effect on both the sol structure and the porosity of the corresponding xerogel. The relation between the pore structure and the AR was investigated for BTESE-based materials in [36].

We studied the formation of a porous structure with SAXS during drying of a sol with AR=0.01 and HR=4. The same initial sol structure but with HR=1 has been studied in [36]. The horizontal geometry of high-intensity synchrotron radiation beamlines that are required to obtain the appropriate time-resolution for *in-situ* studies imposes vertical mounting of samples. To study the drying process of the liquid sol, a specially designed setup was used, in which the drying sol was contained in a rotating cylinder with a Kapton window. The drying liquid was evenly distributed by means of the centrifugal force. Solvent evaporation led to concentration of the colloids. This gave a lower X-ray scattering contrast, reducing the (background-corrected) scattering intensity and concomitantly increasing the statistical noise (Fig. 4). The scattering intensity I is measured as a function of the absolute value of the scattering vector q. The exponent β of the power-law relation

$$I \sim e^{-\beta} \tag{6}$$

that was fitted to the patterns dropped from > 1 to 0.5 within 1 h. At this point all solvent had evaporated from the dry sample and the profile remained unchanged. While β is often referred to as a 'fractal dimension', the power-law relation should technically extend over several orders of magnitude to use this expression. The decrease in electron density contrast can be interpreted as due to the formation of a material that is more homogeneous on the studied length scale (≈ 1–10 nm). As a comparison, the scattering pattern of a similarly *in-situ* dried sample with HR=1 is plotted in Fig. 4. While this pattern had been obtained after 4.5 ks at RT, similar final patterns were found at HR=1 after (faster) drying at 333 K. This latter material can be considered as fully homogenous on the studied length scale. In this pattern, the value of β is even negative, which is related to scattering as a result of local and thermal density fluctuations [55]. As these short-range fluctuations are most prominent at the atomic scale, the scattering intensity increases towards higher q. For the materials with HR=4, other structural arrangements result in relatively strong scattering that obscures these short-range density fluctuations. The remaining electron density contrast strongly indicates that some additional porosity is formed at higher HR, which is in line with the observations on pure SiO_2.

As a more condensed network is formed faster from a more reactive sol, a high-viscosity material ('gel') is also formed in an earlier stage. To investigate how the higher degree of condensation of a more reactive drying sol is related to a higher porosity after solvent evaporation, we studied a BTESE-based sol, prepared with AR=0.1, that was split into three parts. To one part extra water was added to obtain a sol with HR=1.56 (sol 1), while the same volume of ethanol was added to the other parts (sol 2 and 3), which thus remained at HR=1. To obtain a porosity of the corresponding xerogel that was sufficiently high for reliable experimental comparison, the sol samples were further aged in a closed container at 333 K. In a material with a very dense pore structure, diffusion limitations would rather lead to very small and unreliable values in a subsequent gas adsorption experiment. After sol ageing, the containers 1 and 3 were opened simultaneously around the gel point of sol 1 (the one with HR=1.56), while container 2 was opened somewhat later, around its own gel point. After drying and thermal consolidation, the pore structure was studied with N_2 adsorption. The pore volume, surface area and mean pore diameter (calculated from the former two values) of xerogel 1 were higher than those of xerogel 3 (Table 4). Interestingly, the pore structure of xerogels 1 and 2 were more similar. The SAXS patterns (Fig. 5) confirm the higher porosity by a higher electron density contrast of 1 and 2. This experiment compares in slow motion the formation of a porous structure upon dip-coating a sol with a higher HR to one with a lower HR. The water-richer sol 1 gelled earlier than sol 3 and exhibited a more open pore structure. However, as both the mechanical properties of the sol and the resulting pore structures of 1 and 2 were more similar, this experiment also suggests a relation between these properties. While the network strength increases continuously during drying as the result of increasingly rapid condensation reactions, a higher-strength material is formed from a faster reacting sol. The

Table 4
Pore volume and surface area of xerogels from BTESE-based sols with different effective HR determined by N_2 adsorption at 77 K, and mean pore diameter d_p calculated from these values. The onset of drying of sol 1 and 2 was around their respective gel points.

Xerogel	AR=0.1	v_p [cm^3 g^{-1}]	s.a. [m^2 g^{-1}]	d_p [nm]
1	HR=1.56	0.421	909	1.85
2	HR=1	0.418	874	1.91
3	HR=1, dried with sol 1	0.342	817	1.67

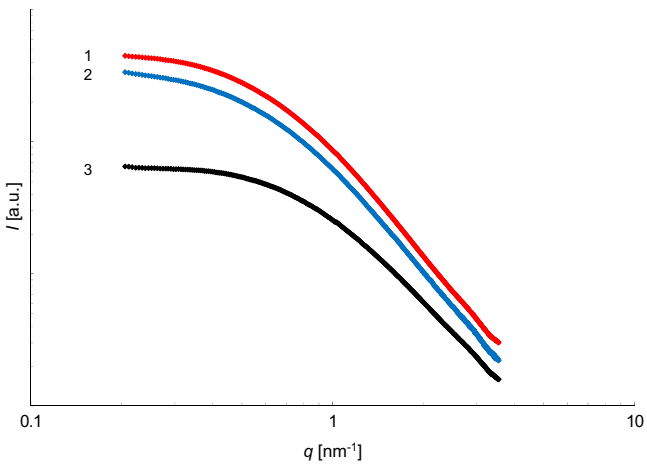

Fig. 5. SAXS patterns of thermally treated unsupported xerogels 1 (AR=0.1, HR=1.56), 2 and 3 (both AR=0.1, HR=1). The onset of drying of 1 and 2 was around their respective gel points, while that of 3 was simultanous with that of 1. The patterns have been shifted vertically relative to each other for better clarity.

strength of a material with a higher (acid and/or water) concentration will therefore be higher at the point when the solvent recedes from the network, resulting in larger pores. This makes a higher HR the indirect cause of a larger pore size, similar as for a higher AR as reported in [36].

3.4. Discussion

As indicated above, a stronger network is formed as the result of a higher degree of condensation and cross-linking of the silica sol moieties, and results in larger pores after drying. The formation of stronger sol networks in the presence of more water can be explained by two effects. Firstly, as water acts as a reactant to hydrolysis, more ethoxy groups are available for polymerization (condensation) reactions. Secondly, as the vapor pressure of water is lower than that of the ethanol solvent, the drying sol becomes enriched in water, and dries at a lower rate. In the additional time, more condensation reactions can occur that strengthen the structure. The stronger structure better resists the increasing capillary forces induced by the receding solvent, resulting in less structural shrinkage and in larger pores. It is thus plausible that the presence of water in the mesopores of the support has a pore-dilating effect in the selective hybrid silica layer.

The degree up to which the material strengthens depends on the condensation rate (related to the concentration of the reactants, including water and acid), and the solvent evaporation rate (which depends on the thickness of the deposited layer and on the type of solvent). Indeed, a lower porosity has been reported at higher drying rates while drying under vacuum, which induces a denser material than drying under ambient conditions [56]. Deposited thin layers also dry faster than the orders of magnitude thicker unsupported materials. This is the reason that overall smaller pores – sizes in the order of small gas molecules, 0.3 to 0.5 nm – are observed in the thin membrane layers than the 1.5–2 nm in the unsupported BTESE-based materials. The relative effects of the acid and hydrolysis ratios, however, can be assumed the same.

In the same way, sol ageing prior to thin film deposition leads to a higher pore volume and larger pores [57]. However, for thin-film coating, only very limited sol ageing can be applied as a certain (minimum and maximum) degree of particle size development is required to allow the formation of a suitable defect-free layer, as explained in Section 3.1. The pore size can thus be tuned far more easily by adapting the composition and reactivity of the dip-sol.

It now becomes clear that the limitation in the H_2/N_2 permselectivity to ≈ 25 of membranes from BTESE-based sols at AR=0.01 as studied in [36] are very likely related to the presence of water in the pores of the support system. To obtain small pores, both the acid and the water content thus need to be restricted. To fabricate membranes with pores suitable for size-based molecular separation of small gas molecules, controlling the dip-coating conditions is therefore essential. Our results indicate that this involves applying a drying procedure of the support system prior to dip-coating. The clearly lower N_2 and CH_4 permeances are now in line with the overall findings in Ref. [36] that showed a decreasing pore size at lower AR. As the amount of acid present during drying of the sol can be varied more easily, it is therefore recommended to carry out pore size tuning by varying the AR, while a dry support system can be regarded as a prerequisite to obtain small pores.

The amount of water and acid present during gelation/drying thus determines the gas permeation cut-off, which is larger than CO_2 for all studied membranes. Still, the minimum attainable pore size is clearly below the kinetic diameter of N_2. The present results thus provide more nuance to the computational studies that suggested that substantial N_2 permeation could occur through ethane-bridged organosilica materials [37,38].

It can be argued that the higher overall H_2/X gas permselectivities reported for membranes prepared from TEOS [14,17] are partly related to the relatively low network formation rate of this precursor compared to BTESE [58]. A lower connectivity of silane moieties before evaporation of most of the solvent suppresses the formation of larger pores. The present results now show that, by careful control of the reactivity by applying both low acid and low water concentrations during membrane fabrication, high gas separation selectivity can also be obtained for BTESE-based hybrid silica membranes. Small molecules such as hydrogen and CO_2 can thus be separated from larger ones, including N_2 and methane. Although the procedure seems to offer room for further optimization, care should be taken that the conditions remain acid-catalyzed, *i.e.* below the isoelectric point (IEP). Above the IEP (*i.e.* at very low AR), the system may become base-catalyzed, resulting in larger pore structures instead.

The single gas permeation results indicate a strong size-based molecular sieving effect, which holds promise for realistic gas separation applications. Examples for relevant industrial applications would for instance be H_2 purification, separation of CO_2 from N_2 in post-combustion processes, and CO_2/CH_4 separation in bio- and natural gas treatment. Considering that many realistic gas mixtures contain substantial amounts of water, gas processing with BTESE-based membranes could offer a promising method in view of their excellent hydrothermal stability [25,34,35].

4. Conclusions

Highly size-selective hybrid silica membranes were prepared by applying a BTESE-based sol with a low acid concentration (H^+:Si=0.01) under controlled dip-coating conditions. Application of well-dried support systems resulted in high size selectivity for gas

permeation. The membranes showed excellent permselectivity of hydrogen and CO_2 to bigger gases, which was almost an order of magnitude higher than those reported in earlier studies. The permselectivities varied for H_2/N_2 between 50 and >400 and for CO_2/CH_4 between 15 and >100. Support systems that had been pretreated at 90% RH prior to coating gave H_2/N_2 permselectivities not exceeding 10. Water adsorbed in the support was assumed to diffuse into the dip-sol and act as a reactant, enhancing condensation during the drying step. Investigation of the drying process with *in-situ* SAXS indicated the formation of a higher porosity for systems in which more water was present. More extensive condensation was concluded to result in a stronger network that exhibits less shrinkage during drying. This gives a structure with larger pores. Under the applied low-acid conditions, careful restriction of the water content in the support is therefore essential to obtain highly size-selective microporous inorganic and hybrid silica membranes from a dip-sol. The combination of the present results with those in an earlier report presents extensive opportunities to fine-tune the properties of hybrid silica membranes for a choice of separations.

Acknowledgments

This research is supported by the Dutch Technology Foundation STW, which is part of the Netherlands Organisation for Scientific Research (NWO), and which is partly funded by the Ministry of Economic Affairs. Mark Smithers (Laboratory for Materials Characterization at the MESA+ Institute of Nanotechnology) is acknowledged for capturing high-resolution SEM images. We thank the Netherlands Organisation for Scientific Research (NWO) for providing us with the possibility of performing SAXS measurements at DUBBLE, and Giuseppe Portale and Wim Bras at DUBBLE for on-site assistance. Rogier Besselink, Tomasz Stawski, Sjoerd Veldhuis and Andre ten Elshof of the Inorganic Materials Science group at the University of Twente are acknowledged for experimental support with the *in-situ* drying experiments.

Nomenclature

List of abbreviations and symbols used throughout the text

AR	acid ratio, H^+:Si
HR	hydrolysis ratio, H_2O:–OC_2H_5
RH	relative humidity
d_{hyd}	mean hydrodynamic diameter determined with dynamic light scattering
d_p	pore diameter determined from gas adsorption
v_p	pore volume determined from gas adsorption
F_i	permeance of gas i
F_i/F_{H_2}	normalized permeance
Δp	gas pressure difference over the membrane
I	scattering intensity
q	absolute value of the scattering vector
β	exponent from power-law relation $I \sim q^{-\beta}$ fitted to a SAXS pattern

References

[1] F. Lipnizki, Cross-flow membrane applications in the food industry, in: K.-V Peinemann, S. Pereira Nunes, L. Giorno (Eds.), Membrane Technology, Membranes for Food Applications, Vol. 3, KGaA,Weinheim, WILEY-VCH Verlag GmbH & Co., 2010.
[2] D. Avnir, T. Coradin, O. Lev, J. Livage, Recent bio-applications of sol–gel materials, J. Mater. Chem. 16 (2006) 1013–1030.
[3] O. Lefebvre, R. Moletta, Treatment of organic pollution in industrial saline wastewater: a literature review, Water Res. 40 (2006) 3671–3682.
[4] L.S. White, Development of large-scale applications in organic solvent nanofiltration and pervaporation for chemical and refining processes, J. Membr. Sci. 286 (2006) 26–35.
[5] S. Sommer, T. Melin, Performance evaluation of microporous inorganic membranes in the dehydration of industrial solvents, Chem. Eng. Process.: Process Intensif. 44 (2005) 1138–1156.
[6] A.M. Urtiaga, E.D. Gorri, P. Gómez, C. Casado, R. Ibáñez, I. Ortiz, Pervaporation technology for the dehydration of solvents and raw materials in the process industry, Dry. Technol. 25 (2007) 1819–1828.
[7] L.M. Vane, A review of pervaporation for product recovery from biomass fermentation processes, J. Chem. Technol. Biotechnol. 80 (2005) 603–629.
[8] L. Deng, M.-B. Hägg, Techno-economic evaluation of biogas upgrading process using CO_2 facilitated transport membrane, Int. J. Greenh. Gas Control 4 (2010) 638–646.
[9] P. Vandezande, L.E.M. Gevers, I.F.J. Vankelecom, Solvent resistant nanofiltration: separating on a molecular level, Chem. Soc. Rev. 37 (2008) 365–405.
[10] L. Lin, Y. Zhang, Y. Kong, Recent advances in sulfur removal from gasoline by pervaporation, Fuel 88 (2009) 1799–1809.
[11] N. Du, H.B. Park, G.P. Robertson, M.M. Dal-Cin, T. Visser, L. Scoles, M.D. Guiver, Polymer nanosieve membranes for CO_2-capture applications, Nat. Mater. 10 (2011) 372–375.
[12] D.F. Stamatialis, B.J. Papenburg, M. Gironés, S. Saiful, S.N.M. Bettahalli, S. Schmitmeier, M. Wessling, Medical applications of membranes: drug delivery, artificial organs and tissue engineering, J. Membr. Sci. 308 (2008) 1–34.
[13] G. Jeon, S.Y. Yang, J.K. Kim, Functional nanoporous membranes for drug delivery, J. Mater. Chem. 22 (2012) 14814–14834.
[14] R.W. Baker, Membrane Technology and Applications, John Wiley & Sons, Ltd., West Sussex, England, 2004.
[15] R.J.R. Uhlhorn, M.H.B.J. Huis In't Veld, K. Keizer, A.J. Burggraaf, Synthesis of ceramic membranes, J. Mater. Sci. 27 (1992) 527–537.
[16] C.J. Brinker, N.K. Raman, M.N. Logan, R. Sehgal, R.-A. Assink, D.-W. Hua, T. L. Ward, Structure property relationships in thin films and membranes, J. Sol-Gel Sci. Technol. 4 (1995) 117–133.
[17] R.M. de Vos, H. Verweij, High-selectivity, high-flux silica membranes for gas separation, Science 279 (1998) 1710–1711.
[18] J. Campaniello, C.W.R. Engelen, W.G. Haije, P.P.A.C. Pex, J.F. Vente, Long-term pervaporation performance of microporous methylated silica membranes, Chem. Commun. (2004) 834–835.
[19] V. Boffa, D.H.A. Blank, J.E. ten Elshof, Hydrothermal stability of microporous silica and niobia–silica membranes, J. Membr. Sci. 319 (2008) 256–263.
[20] K. Yoshida, Y. Hirano, H. Fujii, T. Tsuru, M. Asaeda, Hydrothermal stability and performance of silica–zirconia membranes for hydrogen separation in hydrothermal conditions, J. Chem. Eng. Jpn. 34 (2001) 523–530.
[21] R. Igi, T. Yoshioka, Y.H. Ikuhara, Y. Iwamoto, T. Tsuru, Characterization of Co-doped silica for improved hydrothermal stability and application to hydrogen separation membranes at high temperatures, J. Am. Ceram. Soc. 91 (2008) 2975–2981.
[22] J. Wang, T. Tsuru, Cobalt-doped silica membranes for pervaporation dehydration of ethanol/water solutions, J. Membr. Sci. 369 (2011) 13–19.
[23] H.L. Castricum, A. Sah, M.C. Mittelmeijer-Hazeleger, C. Huiskes, J.E. ten Elshof, Microporous structure and enhanced hydrophobicity in methylated SiO_2 for molecular separation, J. Mater. Chem. 17 (2007) 1509–1517.
[24] R.M. de Vos, W.F. Maier, H. Verweij, Hydrophobic silica membranes for gas separation, J. Membr. Sci. 158 (1999) 277–288.
[25] H.L. Castricum, A. Sah, R. Kreiter, D.H.A. Blank, J.F. Vente, J.E. ten Elshof, Hybrid ceramic nanosieves: stabilizing nanopores with organic links, Chem. Commun. (2008) 1103–1105.
[26] H.L. Castricum, R. Kreiter, H.M. van Veen, D.H.A. Blank, J.F. Vente, J.E. ten Elshof, High-performance hybrid pervaporation membranes with superior hydrothermal and acid stability, J. Membr. Sci. 324 (2008) 111–118.
[27] M. Kanezashi, K. Yada, T. Yoshioka, T. Tsuru, Design of silica networks for development of highly permeable hydrogen separation membranes with hydrothermal stability, J. Am. Chem. Soc. 131 (2009) 414–415.
[28] H.L. Castricum, G.G. Paradis, M.C. Mittelmeijer-Hazeleger, R. Kreiter, J.F. Vente, J.E. ten Elshof, Tailoring the separation behavior of hybrid organosilica membranes by adjusting the structure of the organic bridging group, Adv. Funct. Mater. 21 (2011) 2319–2329.
[29] H.F. Qureshi, A. Nijmeijer, A.J.A. Winnubst, Influence of sol–gel process parameters on the micro-structure and performance of hybrid silica membranes, J. Membr. Sci. 446 (2013) 19–25.
[30] V. Meynen, H.L. Castricum, A. Buekenhoudt, Class II hybrid organic–inorganic membranes creating new versatility in separations, Curr. Org. Chem. 18 (2014) 2334–2350.
[31] A.C. Pierre, Introduction to Sol–Gel Processing, Kluwer Academic Publishers, Boston, USA, 1998.
[32] C.J. Brinker, G.W. Scherer, Sol–gel Science: The Physics and Chemistry of Sol–Gel Processing, Academic Press Ltd., San Diego, USA, 1990.
[33] R.K. Iler, The Chemistry of Silica, Wiley & Sons Inc., New York, USA, 1979.
[34] H.M. van Veen, M.D.A. Rietkerk, D.P. Shanahan, M.M.A. van Tuel, R. Kreiter, H. L. Castricum, J.E. ten Elshof, J.F. Vente, Pushing membrane stability boundaries with HybSi® pervaporation membranes, J. Membr. Sci. 380 (2011) 124–131.

[35] I. Agirre, P.L. Arias, H.L. Castricum, M. Creatore, J.E. ten Elshof, G.G. Paradis, P.H. T. Ngamou, H.M. van Veen, J.F. Vente, Hybrid organosilica membranes and processes: status and outlook, Sep. Purif. Technol. 121 (2014) 2–12.
[36] H.L. Castricum, G.G. Paradis, M.C. Mittelmeijer-Hazeleger, W. Bras, G. Eeckhaut, J.F. Vente, G. Rothenberg, J.E. ten Elshof, Tuning the nanopore structure and separation behavior of hybrid organosilica membranes, Microporous Mesoporous Mater. 185 (2014) 224–234.
[37] K.S. Chang, T. Yoshioka, M. Kanezashi, T. Tsuru, K.L. Tung, Molecular simulation of micro-structures and gas diffusion behavior of organic–inorganic hybrid amorphous silica membranes, J. Membr. Sci. 381 (2011) 90–101.
[38] K.S. Chang, T. Yoshioka, M. Kanezashi, T. Tsuru, K.L. Tung, A molecular dynamics simulation of a homogeneous organic–inorganic hybrid silica membrane, Chem. Commun. 46 (2010) 9140–9142.
[39] G.Z. Cao, J. Meijerink, H.W. Brinkman, A.J. Burggraaf, Permporometry study on the size distribution of active pores in porous ceramic membranes, J. Membr. Sci. 83 (1993) 221–235.
[40] M.G. Kaganer, A new method for the determination of the specific adsorption surface of adsorbents and other finely dispersed substances, Zh. Fiz. Khim. 33 (1959) 2202–2210.
[41] S.J. Gregg, K.S.W. Sing, Adsorption, Surface Area and Porosity, Academic Press, London, UK, 1982.
[42] W. Bras, I.P. Dolbnya, D. Detollenaere, R. v anTol, M. Malfois, G.N. Greaves, A.J. Ryan, E. Heeley, Recent experiments on a combined small-angle/wide-angle X-ray scattering beam line at the ESRF, J. Appl. Crystallogr. 36 (2003) 791–794.
[43] T.M. Stawski, S.A. Veldhuis, H.L. Castricum, E.G. Keim, G. Eeckhaut, W. Bras, D.H.A. Blank, J.E. ten Elshof, Development of nanoscale inhomogeneities during drying of sol–gel derived amorphous lead zirconate titanate precursor thin films, Langmuir 27 (2011) 11081–11089.
[44] H.L. Castricum, A. Sah, R. Kreiter, D.H.A. Blank, J.F. Vente, J.E. ten Elshof, Hydrothermally stable molecular separation membranes from organically linked silica, J. Mater. Chem. 18 (2008) 2150–2158.
[45] R. Kreiter, M.D.A. Rietkerk, H.L. Castricum, H.M. van Veen, J.E. ten Elshof, J.F. Vente, Evaluation of hybrid silica sols for stable microporous membranes using high-throughput screening, J. Sol-Gel Sci. Technol. 57 (2011) 245–252.
[46] M. Kanezashi, K. Yada, T. Yoshioka, T. Tsuru, Organic–inorganic hybrid silica membranes with controlled silica network size: preparation and gas permeation characteristics, J. Membr. Sci. 348 (2010) 310–318.
[47] G. Li, T. Niimi, M. Kanezashi, T. Yoshioka, T. Tsuru, Equilibrium shift of methylcyclohexane dehydrogenation in a thermally stable organosilica membrane reactor for high-purity hydrogen production, Int. J. Hydrog. Energy 38 (2013) 15302–15306.
[48] T. Niimi, H. Nagasawa, M. Kanezashi, T. Yoshioka, K. Ito, T. Tsuru, Preparation of BTESE-derived organosilica membranes for catalytic membrane reactors of methylcyclohexane dehydrogenation, J. Membr. Sci. 455 (2014) 375–383.
[49] B.N. Nair, W.J. Elferink, K. Keizer, H. Verweij, Sol–gel synthesis and characterization of microporous silica membranes I: SAXS study on the growth of polymeric structures, J. Colloid Interface Sci. 178 (1996) 565–570.
[50] W.J. Elferink, B.N. Nair, R. de Vos, K. Keizer, H. Verweij, Sol–gel synthesis and characterization of microporous silica membranes II: tailor-making porosity, J. Colloid Interface Sci. 180 (1996) 127–134.
[51] C.A. Aerts, E. Verraedt, A. Depla, L. Follens, L. Froyen, J. Van Humbeeck, P. Augustijns, G. Van den Mooter, R. Mellaerts, J.A. Martens, Potential of amorphous microporous silica for ibuprofen controlled release, Int. J. Pharm. 397 (2010) 84–91.
[52] R.F.S. Lenza, W.L. Vasconcelos, Synthesis and properties of microporous sol–gel silica membranes, J. Non-Cryst. Solids 273 (2000) 164–169.
[53] R.S.A. De Lange, J.H.A. Hekkink, K. Keizer, A.J. Burggraaf, Polymeric-silica-based sols for membrane modification applications: sol–gel synthesis and characterization with SAXS, J. Non-Cryst. Solids 191 (1995) 1–16.
[54] B.N. Nair, J.W. Elferink, K. Keizer, H. Verweij, Preparation and structure of microporous silica membranes, J. Sol-Gel Sci. Technol. 8 (1997) 471–475.
[55] R.-J. Roe, Methods of X-ray and Neutron Scattering in Polymer Science, Oxford University Press, New York, USA, 2000.
[56] R.S.A. De Lange, K-N.P. Kumar, J.H.A. Hekkink, G.M.H. van de Velde, K. Keizer, A.J. Burggraaf, W.H. Dokter, H.F. van Garderen, T.P.M. Beelen, Microporous SiO_2 and SiO_2/MO_x (M=Ti, Zr, Al) for ceramic membrane applications: a microstructural study of the sol-stage and the consolidated state, J. Sol-Gel Sci. Technol. 2 (1994) 489–495.
[57] C.J. Brinker, R. Sehgal, S.L. Hietala, R. Deshpande, D.M. Smith, D. Loy, C. S. Ashley, Sol–gel strategies for controlled porosity inorganic materials, J. Membr. Sci. 94 (1994) 85–102.
[58] H.L. Castricum, A. Sah, J.A.J. Geenevasen, R. Kreiter, D.H.A. Blank, J.F. Vente, J. E. ten Elshof, Structure of hybrid organic–inorganic sols for the preparation of hydrothermally stable membranes, J. Sol-Gel Sci. Technol. 48 (2008) 11–17.